remote sensing

MDPI

Article

Spatio-Temporal Patterns of NDVI and Its Influencing Factors Based on the ESTARFM in the Loess Plateau of China

Xinyi Fan [1], Peng Gao [1,2,3,*], Biqing Tian [1], Changxue Wu [1] and Xingmin Mu [1,2,3]

[1] Regional Soil and Water Conservation and Environmental Effects Research Department, Institute of Soil and Water Conservation, Northwest A&F University, Xianyang 712100, China
[2] Institute of Soil and Water Conservation, Chinese Academy of Sciences and Ministry of Water Resources, Xianyang 712100, China
[3] University of Chinese Academy of Sciences, Beijing 100049, China
* Correspondence: gaopeng@ms.iswc.ac.cn

Abstract: The Loess Plateau is ecologically vulnerable. Vegetation is the key factor in ecological improvement. The study of the distribution patterns of vegetation and its impact factors has important guiding meaning for ecological construction in the region. The existing single sensor cannot provide long-term and high-resolution data. We established data of NDVI with a great spatial resolution by fusing the GIMMS NDVI and the MODIS NDVI based on the ESTARFM. Furthermore, we analyzed the variation in NDVI under different topographies and its response to climatic factors and human activities in the Loess Plateau. The results manifested that: (1) The fused NDVI by the ESTARFM had a high correlation with the MODIS NDVI and can be used in subsequent studies. (2) The multi-year average NDVI of this region ranged from 0.027 to 0.973, which is specifically low in the northwest and high southeast. The NDVI manifested an upward trend in the last 31 years. Its growth rate was 0.0036/a ($p < 0.01$). Spatially, the area with an upward trend of NDVI accounted for 89.48% of the plateau. (3) For topography, the larger area with the extremely significant upward of NDVI was found at elevations of 500–1500 m, with slopes of 6–15°. The larger area with the extremely significant downward trend of NDVI was found at an elevation of higher than 3000 m, with a slope of greater than 35°. (4) The response of the NDVI to the climatic factors manifested a significant spatial heterogeneity. The temperature had a more significant impact on NDVI than precipitation. (5) Human activities contributed more to NDVI than climatic factors (65.22% for human activities and 34.78% for climatic factors). Among them, the area with a high contribution of human activities to NDVI increase was consistent with the area where the GGP was implemented. The distribution of areas with high contribution of human activities to NDVI decrease was in line with that of the provincial capital cities. The results served as the theoretical foundation for assessing the efficacy of environmental stewardship and for optimizing ecological restoration measures.

Keywords: NDVI; ESTARFM; climatic factors; topography; human activities

check for updates

Citation: Fan, X.; Gao, P.; Tian, B.; Wu, C.; Mu, X. Spatio-Temporal Patterns of NDVI and Its Influencing Factors Based on the ESTARFM in the Loess Plateau of China. *Remote Sens.* **2023**, *15*, 2553. https://doi.org/10.3390/rs15102553

Received: 15 March 2023
Revised: 7 May 2023
Accepted: 9 May 2023
Published: 13 May 2023

Copyright: © 2023 by the authors. Licensee MDPI, Basel, Switzerland. This article is an open access article distributed under the terms and conditions of the Creative Commons Attribution (CC BY) license (https://creativecommons.org/licenses/by/4.0/).

1. Introduction

A critical constituent of the terrestrial ecosystem is vegetation; it is momentous for the flow of energy and materials around the world [1]. Moreover, vegetation is so sensitive to environmental variations [2]. Thus, the dynamic changes in vegetation coverage and their link with environmental conditions based on remote sensing can offer scientific evidence for the stability of regional ecology and the formulation of ecological conservation programs.

The great spatial and temporal precision of remote sensing data allows for the large-scale surveillance of vegetation variation [3]. NDVI, as an effective indicator that can monitor the variation of surface vegetation, quantitatively evaluates the regional vegetation coverage and growth status [4,5]. NDVI, with various spatial and temporal resolutions, has been generally applied in desertification evaluations [6], soil erosion monitoring [7], and land-cover changes [8] with the advancement of remote-sensing technology. For instance,

He et al. used GIMMS NDVI3g to map the annual LULC (Land Use and Land Cover) in China [9]. Pan et al. inverted the spatio-temporal dynamic change process of land desertification in the Alxa League from 2000 to 2016 using MODIS NDVI data [10]. Li et al. examined the spatial characteristics of vegetation degradation and its link with urbanization in the Yangtze River Delta using SPOT NDVI [11]. Among them, GIMMS NDVI, provided by the Global Inventory Modeling and Mapping Studies (GIMMS) Advanced Very-High Resolution Radiometer (AVHRR), is the most important data from the 1980s to the present [12]. The advantages of GIMMS NDVI are the wide coverage and long timescale. However, GIMMS NDVI is difficult to capture the detailed features of actual vegetation variations due to low spatial resolutions and severe pixel mixing. MODIS NDVI and SPOT NDVI have greater spatial resolutions than the former. Both data are less affected by atmospheric water vapor. So, the quality of these data has improved. However, the short accumulation times of MODIS NDVI and SPOT NDVI make it difficult to meet the needs of vegetation variation over a long period of time.

The fusion of sensor data with various spectral, temporal, and spatial resolutions is a practical method for the above-mentioned problem. The data fusion methods can be classified into two types: one is based on the transformation model, and the other is based on the pixel reconfiguration model. At present, most existing data fusion models are grounded in pixel reconfiguration techniques. The Spatial and Temporal Adaptive Reflectance Fusion Model (STARFM) is the earliest proposed data fusion model, which was raised by Gao et al. [13]. This model fuses Landsat and MODIS images to establish the data with great spatial and temporal resolutions, taking into consideration the similarities of spectrum and space between image pixels. Yin et al. improved the accuracy of rice mapping using the STARFM [14]. Hilker et al. proposed the Spatial–Temporal Adaptive Algorithm for Mapping Reflectance Change (STAARCH) by improving the STARFM. It can capture the variations in surface vegetation [15]. The ESTARFM was raised by Zhu et al. based on the further perfection of the STARFM [16]. The model not only considered the spectral and spatial similarities between the target and similar pixels but also incorporated the surface reflectance to better describe the characteristics of vegetation. Numerous studies have revealed that the ESTARFM had a higher precision of fusion results than the other spatio-temporal data fusion models in regions with a complex and heterogeneous topography [17,18].

The Loess Plateau is situated in a semi-humid and semi-arid zone. The worst soil erosion and the most fragile ecological environment have made it a priority area for ecological restoration in China because of the fragmented terrain and the undulating topography [19]. Studies of vegetation variation and its impact factors are crucial in this typical ecologically sensitive area. Several researchers have investigated the vegetation variation and its impact factors in this region. These achieved several meaningful results. Li et al. argued that NDVI has significantly increased in recent years [20]. Sun et al. believe that the dynamic changes in vegetation coverage were intimately related to the temperature fluctuation, which was the main influence on the enhancement of vegetation activity [21]. However, previous studies of the dynamic characteristics of NDVI and its impact factors have mostly been conducted with single NDVI data. Few studies used data with a long-time and great spatial resolution. On the other hand, some studies have only considered the response between climatic factors and human activities and NDVI. Topographic factors can influence the regional microclimate differences and human activity frequency through external morphologies, such as elevation and slope, which affect the characteristics of NDVI variation. However, this has been neglected.

We studied the spatio-temporal patterns of NDVI and its influencing factors using the GIMMS NDVI and MODIS NDVI. The specific objectives are: (1) to create new NDVI data with great spatial resolutions by fusing the GIMMS NDVI and MODIS NDVI based on ESTARFM; (2) to analyze the spatio-temporal patterns of NDVI using the fused NDVIs of this plateau; (3) to explore the variation in the NDVI under different topographies and its response to climatic factors and human activities. We hope that this will provide the

theoretical basis and scientific foundation for sustainable ecological development and the formation of future ecological rehabilitation measures.

2. Study Area and Data

2.1. Study Area

The Loess Plateau (33°43′–41°16′N, 100°54′–114°33′E) is situated in the northwestern portion of China. It begins with the Riyue Mountain in the west and extends to the Taihang Mountain in the east. It is bounded by the Yin Mountains in the north and the Qinling Mountains in the south. It spans seven provinces (autonomous regions): Shanxi, Shaanxi, Ningxia, Qinghai, Gansu, Inner Mongolia, and Henan, with approximately 6.24 × 10^5 km^2. The Loess Plateau, located on the second level of China's landforms and the second level of the transition zone to the third level of the terrace, is the world's largest area of loess deposition. The elevation ranges from 12–5232 m, showing a rising trend from the southeast to the northwest. The climate of the Loess Plateau is characterized by a typical monsoon climate. The mean annual temperature is between 4–14 °C, and the annual precipitation is between 200–750 mm in this region. These have a significant geographical heterogeneity, which increases from the northwest to the southeast. Precipitation is mostly concentrated from June to September. According to the climate (temperature, precipitation) and vegetation, the study area can be categorized into five bioclimatic zones (Figure 1) [22].

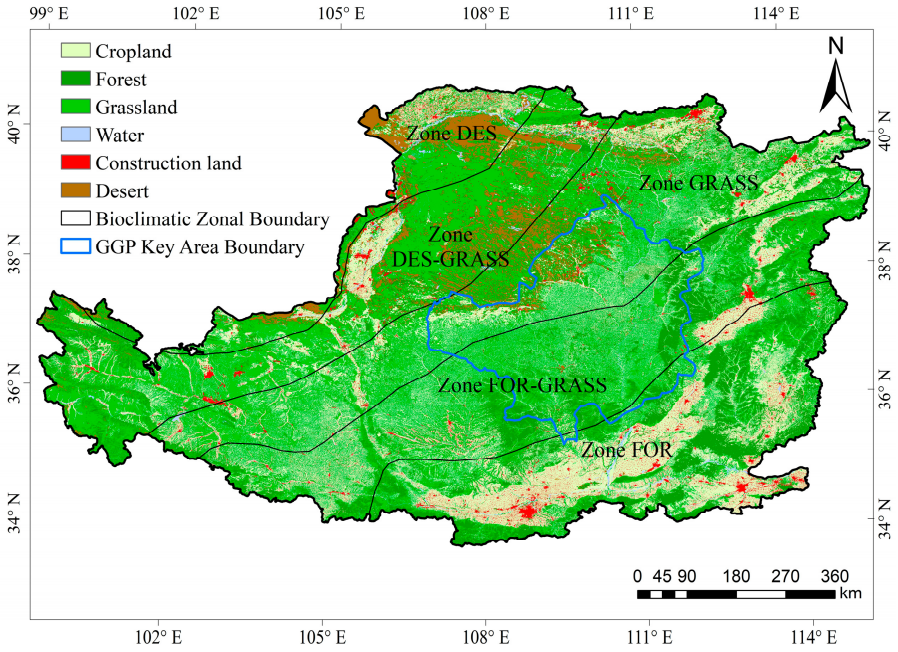

Figure 1. Distribution of land-cover types and different bioclimatic zones in the Loess Plateau: Zone FOR (Forest Zone), Zone FOR-GRASS (Forest-grasslands Zone), Zone GRASS (Typical Grasslands Zone), Zone GRASS-DES (Grasslands-desert Zone), and Zone DES (Deserts Zone).

2.2. Data Collection

2.2.1. NDVI Data

The required NDVI data and their sources, spatio-temporal resolutions, and study period were shown in Table 1.

We used the Savitzky-Goaly (S-G) filtering maximum to smooth the MODIS NDVI to reduce the effects of noise, such as outliers. Then, we used Value Composition (MVC) to generate the year-by-year maximum NDVI in order to reduce the difference in temporal resolutions between the two data and to further eliminate the effects of clouds and atmospheric water vapor. In addition, the GIMMS NDVI was resampled to 250 m in preparation for subsequent data fusion using the ESTARFM model.

Table 1. NDVI data sources, spatio-temporal resolution, and study period.

Data Name	Source	Temporal Resolution	Spatial Resolution	Study Period
MOD13Q1	http://www.gscloud.cn/ (accessed on 10 July 2022)	16 days	250 m	2000–2015
GIMMS	https://ecocast.arc.nasa.gov/data/pub/gimms/3g.v1/ (accessed on 10 July 2022)	15 days	8 km	1985–2015

2.2.2. Climate Data

The climate data were obtained from the Loess Plateau SubCenter, the National Earth System Science Data Center, and the National Science & Technology Infrastructure of China (http://loess.geodat.cn/ (accessed on 2 January 2023)), which included the month-by-month temperature and precipitation from 1985 to 2015. The resolution is 1 km. The raster data of the annual precipitation and annual average temperature were generated separately in Arc GIS to have a similar projection and spatial resolution as NDVI.

2.2.3. Topography Data

The DEM data were sourced from the Geospatial Data Cloud Platform of the Computer Network Information Center of the Chinese Academy of Sciences (https://www.gscloud.cn/ (accessed on 18 December 2022)) with a resolution of 30 m (Figure 2). The slope data were extracted from the DEM data. The spatial resolution of this data was resampled to be compatible with the NDVI.

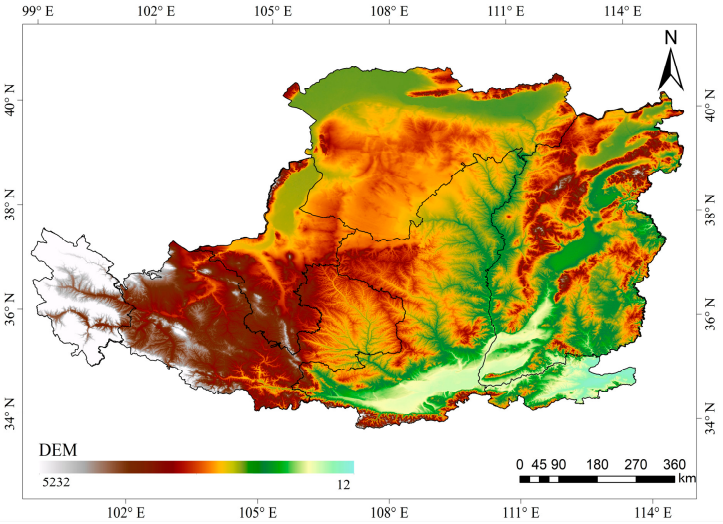

Figure 2. Topography of the Loess Plateau.

2.2.4. Boundary Data

The Loess Plateau vector boundary data were obtained from the Resource and Environment Science Data Center of the Chinese Academy of Sciences (https://www.resdc.cn/ (accessed on 26 May 2022)). The boundaries of the key areas of the GGP were obtained from Zhao et al. [23].

3. Methods

3.1. ESTARFM Fusion Algorithm

The ESTARFM fusion model assigns weight values and conversion coefficients to similar pixels by spatial and spectral similarity. It uses similar pixels to calculate the predicted value of the central pixels to obtain data with a great spatial resolution of the

prediction period [16]. This study used ESTARFM to establish NDVI data with a 250 m-resolution from 1985 to 1999 in the Loess Plateau. The formula is as follows:

$$\mathrm{M}(x_{w/2}, y_{w/2}, \mathrm{t_p}, \mathrm{B}) = \mathrm{M}(x_{w/2}, y_{w/2}, \mathrm{t}_k, \mathrm{B}) + \sum_{\mathrm{i}=1}^{\mathrm{N}} \mathrm{W}_i \times \mathrm{V}_i \times (\mathrm{G}(x_i, y_i, \mathrm{t_p}, \mathrm{B}) - \mathrm{G}(x_i, y_i, \mathrm{t}_k, \mathrm{B}) \quad (1)$$

where M, G are MODIS and GIMMS image data, respectively; w is the size of the sliding window; $(x_{w/2}, y_{w/2})$ is the center position of the pixels to be measured; (x_i, y_i) is the position of the i-th similar pixels; t_k, $\mathrm{t_p}$ are image acquisition times; B is the image band; N is the number of similar pixels; V_i is conversion factor; W_i is the weight value of similar pixels to the central pixels, and its calculation formulas are as follows:

$$\mathrm{W}_i = (1/D_i) / \sum_{i=1}^{\mathrm{N}} (1/D_i) \quad (2)$$

$$D_i = (1 - R_i) \times d_i \quad (3)$$

$$d_i = 1 + \sqrt{(x_{w/2} - x_i)^2 + (y_{w/2} - y_i)^2} / (w/2) \quad (4)$$

where D_i is the product of the spectral similarity and spatial distance calculation of central pixels and similar pixels; R_i is the spectral similarity weight value; d_i is the spatial distance weight value of similar pixels and central pixels.

We choose two pairs of MDOIS and GIMMS data at $\mathrm{t_a}$ and $\mathrm{t_b}$ moments to predict the MODIS $\mathrm{t_p}$ moments by combining the GIMMS data at $\mathrm{t_p}$ moments with Equation (1), and the results were denoted as $\mathrm{M_a}(x_{w/2}, y_{w/2}, \mathrm{t_p}, \mathrm{B})$ and $\mathrm{M_b}(x_{w/2}, y_{w/2}, \mathrm{t_p}, \mathrm{B})$, respectively. We were able to obtain a more accurate $\mathrm{t_p}$ moment reflectance by a weighted combination of these two predictions. This weight is calculated as:

$$T_k = \frac{1 / \left| \sum_{j=1}^{w} \sum_{i=1}^{w} G(x_i, y_j, t_k, B) - \sum_{j=1}^{w} \sum_{i=1}^{w} G(x_i, y_j, t_P, B) \right|}{\sum_{k=a,b} \left(1 / \left| \sum_{j=1}^{w} \sum_{i=1}^{w} G(x_i, y_j, t_k, B) - \sum_{j=1}^{w} \sum_{i=1}^{w} G(x_i, y_j, t_P, B) \right| \right)} \ (k = a, b) \quad (5)$$

The final model that predicted the reflectance of MODIS images in time is calculated as follows:

$$M_{\mathrm{p}}(x_{w/2}, y_{w/2}, \mathrm{t_p}, \mathrm{B}) = T_{\mathrm{a}} M_{\mathrm{a}}(x_{w/2}, y_{w/2}, \mathrm{t_a}, \mathrm{B}) + T_b M_{\mathrm{b}}(x_{w/2}, y_{w/2}, \mathrm{t_b}, \mathrm{B}) \quad (6)$$

All of the above parameters have been mentioned in the previous section.

3.2. Trend Analysis

The linear regression slope can be used as an index to quantitatively assess the dynamic changes in vegetation coverage during the duration of the study [24,25]. We calculated the trend of NDVI from 1985–1999, 2000–2015, and 1985–2015 for each pixel using the least-squares regression method. The calculation equation is as follows:

$$Slope = \frac{n \times \sum_{m=1}^{n} (m \times \mathrm{NDVI}_m) - (\sum_{m=1}^{n} m) \times \sum_{m=1}^{n} \mathrm{NDVI}_m}{n \times \sum_{m=1}^{n} m^2 - (\sum_{m=1}^{n} m)^2} \quad (7)$$

where NDVI_m is the annual maximum NDVI in the m year; n is the number of years in the study period; m is the time variable (an integer from 1 to n). We tested for significance using the F-test, and the results were categorized as 5 types based on the test results (Table 2).

Table 2. Statistically significant categorizations of NDVI variability trend.

Grading Criteria	Degree
Slope > 0, $p < 0.01$	extremely significant upward
Slope > 0, $0.01 \leq p < 0.05$	significant upward
Slope > 0, $p \geq 0.05$	no significant upward
Slope < 0, $p \geq 0.05$	no significant downward
Slope < 0, $0.01 \leq p < 0.05$	significant downward
Slope < 0, $p < 0.01$	extremely significant downward

Notes: Slope is the trend of the NDVI during the study period. Slope > 0 indicates an upward trend of NDVI with time. Slope < 0 indicates a downward trend of NDVI with time. p is the significance level of the F-test. A value of $p < 0.01$ represents a highly significant trend of NDVI variation. $0.01 \leq p < 0.05$ represents a significant trend of NDVI variation. A value of $p \geq 0.05$ represents an insignificant trend of NDVI variation.

3.3. Correlation Analysis

The Pearson Correlation Analysis is a method to study the degree of correlation between the variables. We analyzed the relationship between the NDVI and each climatic factor by calculating the Pearson correlation coefficient between them. The formula is as follows:

$$r_{xy} = \frac{\sum_{i=1}^{n}\left(\mathrm{NDVI}_i - \overline{\mathrm{NDVI}}\right)(y_i - \overline{y})}{\sqrt{\sum_{i=1}^{n}\left(\mathrm{NDVI}_i - \overline{\mathrm{NDVI}}\right)^2 \sum_{i=1}^{n}(y_i - \overline{y})^2}} \quad (8)$$

where n is the total number of years; NDVI_i is the annual maximum NDVI of i-th year; y_i is the average annual temperature or annual precipitation of i-th year; $\overline{\mathrm{NDVI}}$ is the n-year mean annual maximum NDVI; $\overline{y}$ is the average of temperature or precipitation in the study period.

3.4. Residual Analysis

Residual analysis is a measure to distinguish the influence of climate factors and human activities on NDVI. We choose precipitation and temperature to establish a linear regression model between both and NDVI to calculate the NDVI under the influence of precipitation and temperature (Equation (9)). This was the predicted NDVI (NDVI_{CF}). It is used to show the influence of climatic factors on NDVI. The difference between the observed NDVI and NDVI_{CF} was used to express the influence of human activities on NDVI (Equation (10)). The formulas are as follows:

$$\mathrm{NDVI}_{CF} = a \times T + b \times P + c \quad (9)$$

$$\mathrm{NDVI}_{HA} = \mathrm{NDVI} - \mathrm{NDVI}_{CF} \quad (10)$$

where NDVI_{CF} and NDVI represent the predicted NDVI based on regression models and the observed NDVI based on remote sensing images, respectively; a, b and c are the model parameters; T, P represent the annual average temperature and the accumulated precipitation, respectively; NDVI_{HA} is the residual.

4. Results

4.1. Data Fusion and Accuracy Evaluation

We randomly selected the fused image and the MODIS NDVI image in 2010 for a detailed comparison and the scattered points of pixels. The spatial resolution of the fused data was greater than that of the GIMMS NDVI (Figure 3). Additionally, the feature texture of the fused data was similar to that of the MODIS NDVI. For relevance, the scattering of the fused images and MODIS NDVI is essentially spread over the y = x line. The correlation coefficient R^2 between the two data reached 0.93 ($p < 0.01$) (Figure 4). Therefore, the fused images well-captured the spectral information of the MODIS NDVI in the same period. They can be used as a data source to analyze the characteristics of vegetation coverage and

its impact factors. This result also verified the applicability of the ESTARFM model in the Loess Plateau.

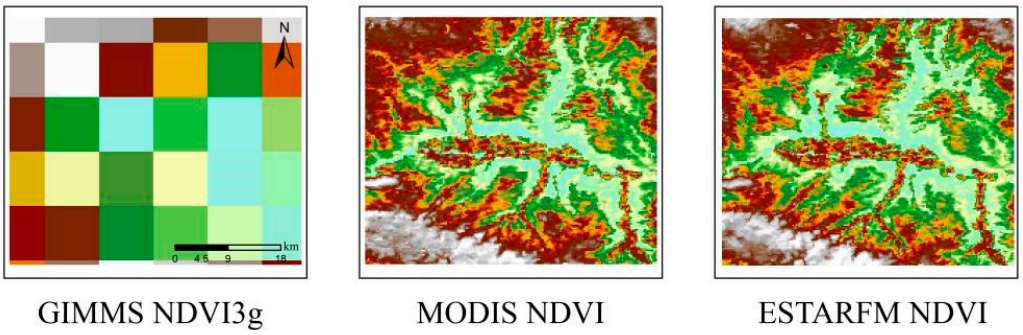

Figure 3. Fusion data comparison.

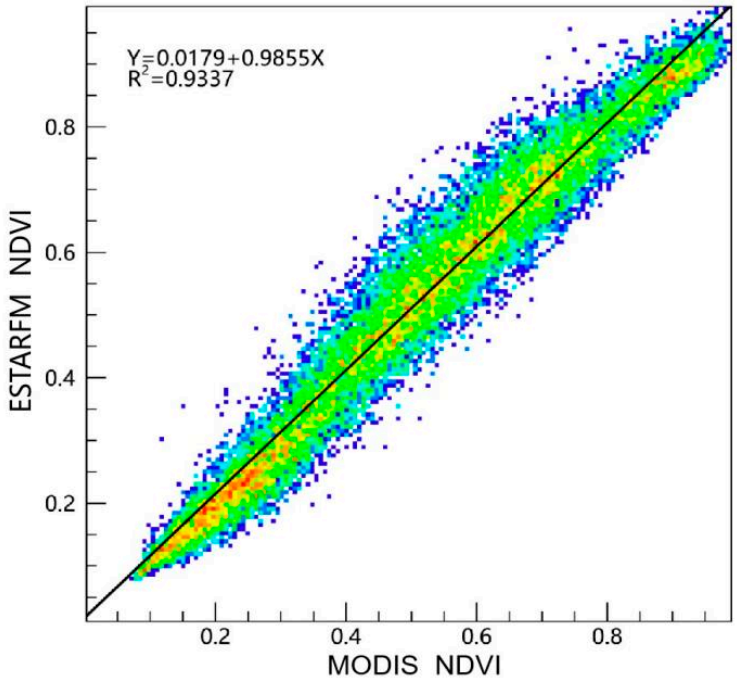

Figure 4. Correlation scatter plot of ESTARFM NDVI and MODIS NDVI.

4.2. Spatial Distribution Characteristics of NDVI

The features of the spatial distribution of the multi-year average maximum NDVI in this plateau are shown in Figure 5. The average NDVI ranged from 0.027 to 0.973, the general pattern of its regional distribution exhibited a downward trend from southeast to northwest. The area where the NDVI was less than 0.3 accounted for 25.15% of this plateau. This was mainly concentrated in the northwestern parts of this plateau. The area where the NDVI was in the range of 0.3–0.5 accounted for 28.81% of this plateau. This was found in stripes from the northeast to the southwest of this plateau, such as southern Ningxia, northern Shaanxi, etc. The area where the NDVI was more than 0.5 accounted for 46.04% of this plateau. This was found in the southeastern part of this plateau. The distribution characteristics of the NDVI were basically similar to the bioclimatic zoning of this plateau. Specifically, the NDVI of Zone FOR was the largest (0.67), while that of Zone DES was the smallest (0.28) (Figure 6).

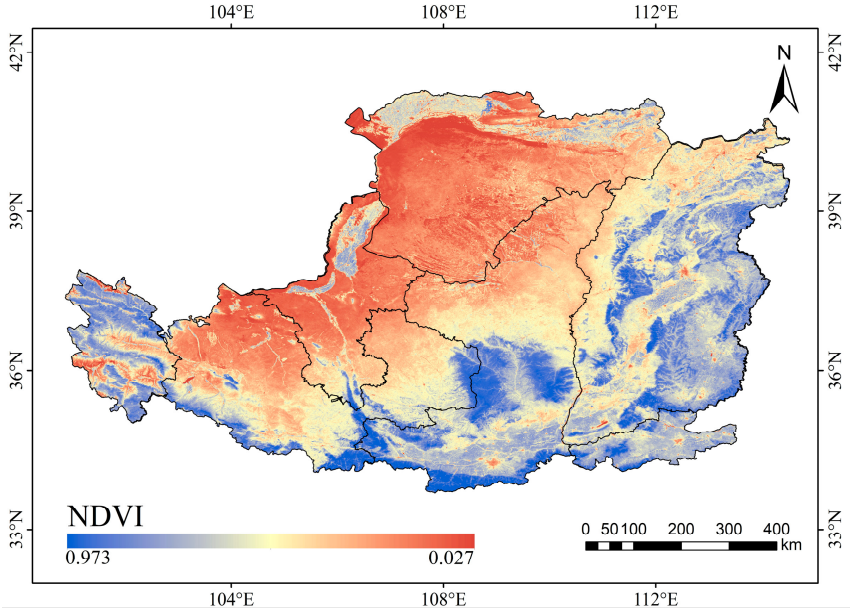

Figure 5. The spatial distribution of maximum multi-year average NDVI in the Loess Plateau.

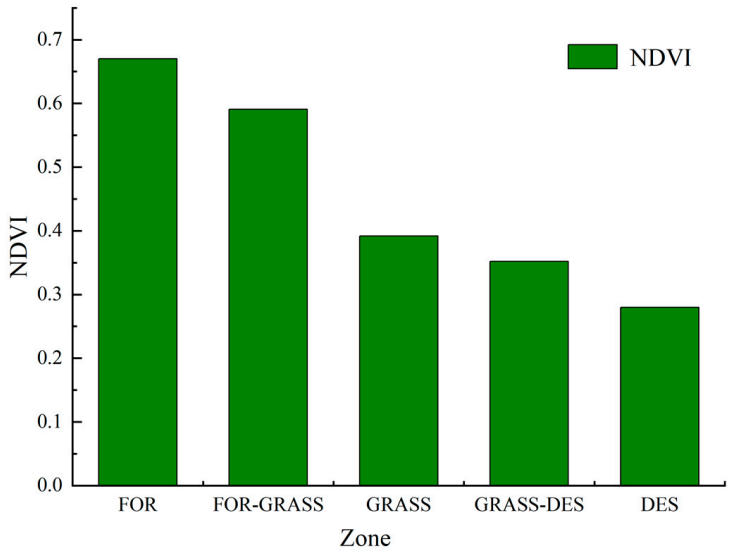

Figure 6. Maximum multi-year average NDVI in different bioclimatic zones.

4.3. Spatio-Temporal Patterns of NDVI

Over the past 31 years, the annual maximum NDVI represented an upward trend in this plateau. Its average interannual variation rate was 0.0036/a ($p < 0.01$). The NDVI has phase characteristics, which can be divided into two phases: the slowly rising phase (1985–1999, with a growth rate of 0.0008/a) and the sharply rising phase (2000–2015, with a growth rate of 0.0078/a) (Figure 7).

Figure 8 demonstrates the spatial distribution patterns of NDVI trends in various periods. The area with an upward trend of the NDVI from 1985 to 1999 accounted for 60.90% of this plateau, in which the area passing the 0.05 significance level test (10.84%) was found in the northern portion of this plateau. Around 39.10% of this plateau presented a downward trend of the NDVI. The area where the NDVI increased from 2000 to 2015 represented 93.18% of this plateau, which was 1.5 times more than the previous period (1985–1999). The area passing the significance level test of 0.05 (67.10%) was located in the northern, middle, and southwestern portions of this plateau, which embraced a high degree of erosion of hilly and gully regions. While only 6.82% of this plateau presented a

downward trend of the NDVI, 89.48% of this plateau presented an upward trend of the NDVI from 1985 to 2015. The area passing the significance level test in the central part of the Loess Plateau is 0.05 (76.67%), which was mainly centralized in the key region of the Grain for Green Project (GGP). Only 10.52% of this plateau presented a downward trend of the NDVI.

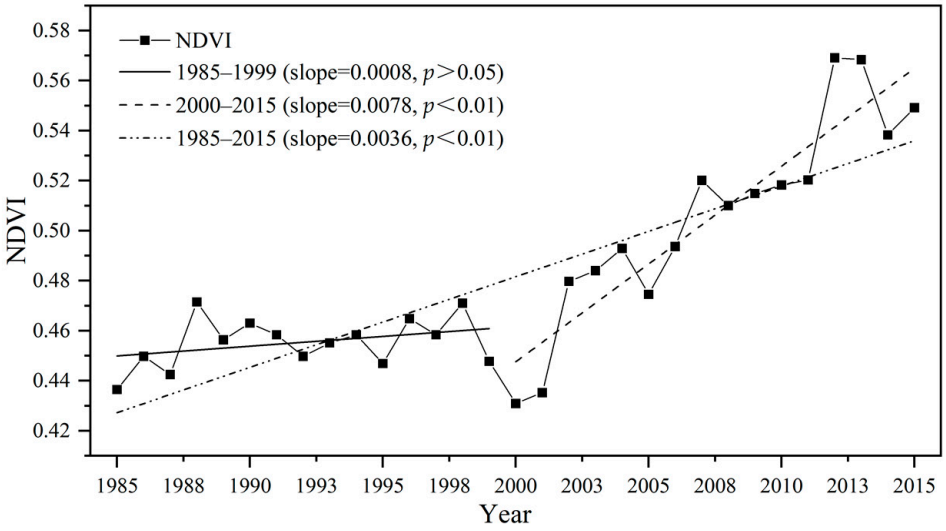

Figure 7. The variation in the maximum annual NDVI of the Loess Plateau in 1985–2015, 1985–1999 and 2000–2015.

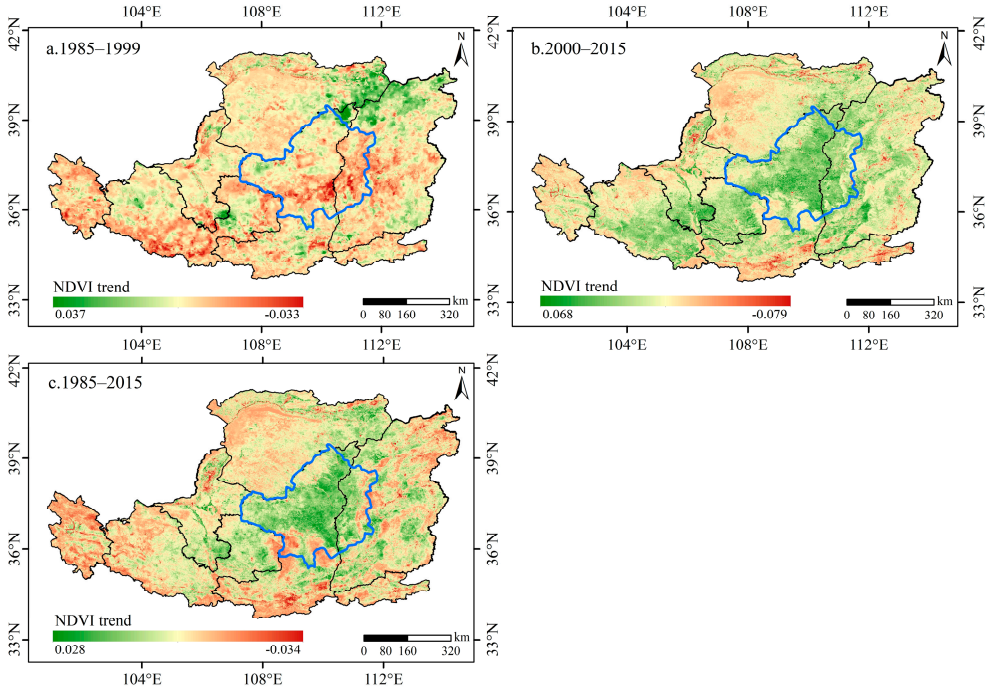

Figure 8. The spatial patterns of NDVI trends in the Loess Plateau. (**a**) From 1985 to 1999, (**b**) 2000 to 2015, and (**c**) 1985 to 2015.

4.4. Topographic Divergence Pattern of NDVI trends

The elevation was divided into nine classes. The slope was divided into five classes, which were extracted using the DEM data (Table 3). Additionally, the change in the trend of NDVI was counted by zoning (Figure 9).

Table 3. Classification range and proportion of elevation and slope in the Loess Plateau.

Elevation Classification/m	Proportion/%	Slope Classification/°	Proportion/%
<500	4.62	<6	33.16
500–1000	12.88	6–15	36.06
1000–1500	51.65	15–25	21.07
1500–2000	18.73	25–35	7.81
2000–2500	6.55	>35	1.90
2500–3000	2.44	-	-
3000–3500	1.73	-	-
3500–4000	1.08	-	-
>4000	0.32	-	-

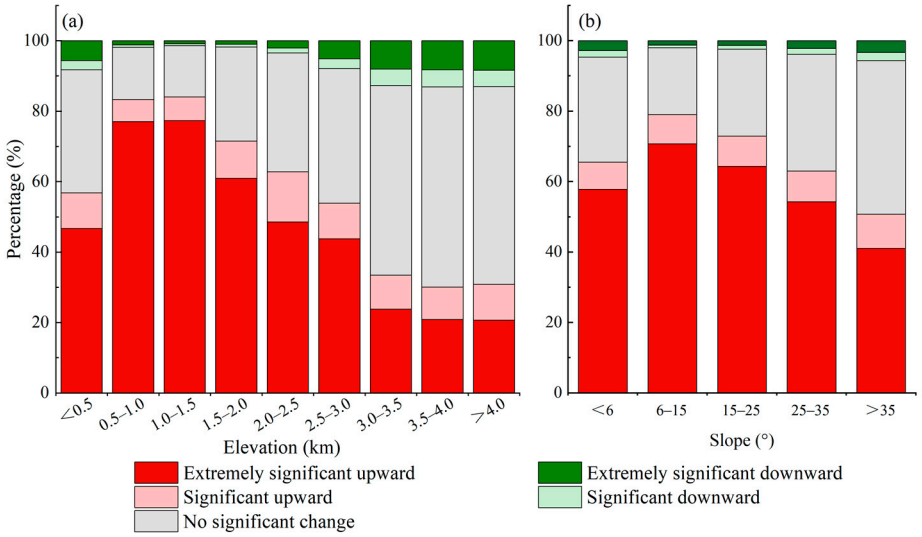

Figure 9. NDVI trend types under different terrain factors in the Loess Plateau. (**a**) Elevation, (**b**) Slope.

The trends of NDVI variation were dominated by two categories of extremely significant upward trends and no significant changes in different elevations and slopes. In terms of elevation, the larger area with the extremely significant upward trend of NDVI was located at elevations of 500–1000 m and 1000–1500 m, accounting for 77.08% and 77.04%, respectively. The larger area with the extremely significant downward trend of NDVI was located at elevations of 3000–3500 m, 3500–4000 m, and >4000 m, accounting for 8.06%, 8.22%, and 8.37%, respectively. For the slope, the larger area with the extremely significant upward trend of NDVI was located at slopes of 6–15°, accounting for 70.74%. The larger area with the extremely significant downward trend of NDVI was found over 35°, accounting for 3.32%.

4.5. The Response of NDVI to Climatic Factors

The interannual trends of temperature and precipitation for this plateau from 1985 to 2015 are shown in Figure 10. The annual average temperature showed an upward trend, with an average change rate of about 0.04 °C/a. The annual precipitation presented a slight upward trend, with an average change rate of about 0.75 mm/a. The average annual temperature and precipitation of this plateau were 8.21 °C and 434.48 mm, respectively. The spatial variability of the average annual temperature and precipitation was significant (Figure 11). Among them, the annual average temperature was high in the southeast and low in the west and northeast. The annual precipitation presented a downward trend from the southeast to the northwest.

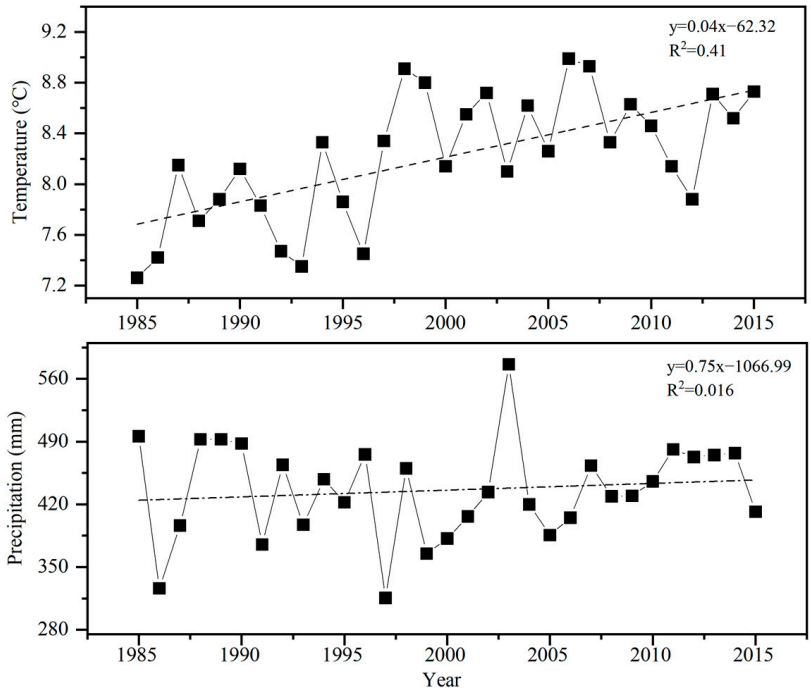

Figure 10. Interannual variation of climatic factors in the Loess Plateau from 1985–2015.

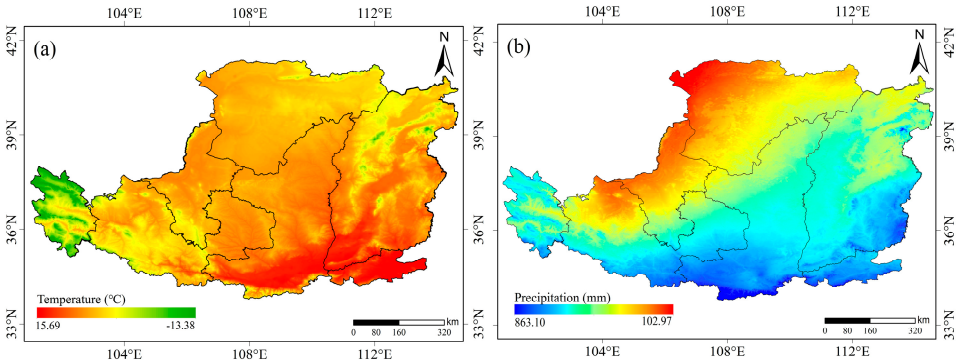

Figure 11. The spatial distribution of climatic factors of the Loess Plateau. (**a**) Temperature, (**b**) Precipitation.

Spatial patterns of the correlation among the annual maximum NDVI with the annual average temperature and annual precipitation are presented in Figure 12. Approximately, 87.85% of this plateau was positively correlated with the temperature in the NDVI, distributed in the northern Shaanxi, Inner Mongolia, Shanxi, and Ningxia. Among them, 35.44% passed the significance level test of 0.05. This was mainly concentrated in the key area of GGP, eastern Inner Mongolia, and southern Shanxi. Around 12.15% of this plateau was negatively correlated with the temperature in the NDVI, which was mainly distributed in Qinghai, western Gansu, southern Shaanxi, and north-central Shanxi. Among them, 5.52% passed the significance level test of 0.05. Around 91.96% of this plateau was positively correlated with the precipitation in the NDVI, distributed in Gansu, southern Ningxia, Inner Mongolia, and northern Shaanxi. Among them, 19.53% passed the significance level test of 0.05. This was mainly concentrated in the Northern Gansu, northeastern Shaanxi, southwestern Ningxia, and northwestern Inner Mongolia. Approximately, 8.04% of this plateau was negatively correlated with precipitation in the NDVI, which was scattered in Qinghai, southern Shaanxi, and northern Shanxi. Among them, only 1.38% passed the significance level test of 0.05. The average correlation coefficients of temperature and precipitation with the annual maximum NDVI were 0.24 and 0.22, respectively. Temperature and precipitation were significantly correlated with the NDVI in 31.81% and 18.05% of

this region. In general, the effect of temperature on the NDVI was greater than that of the precipitation.

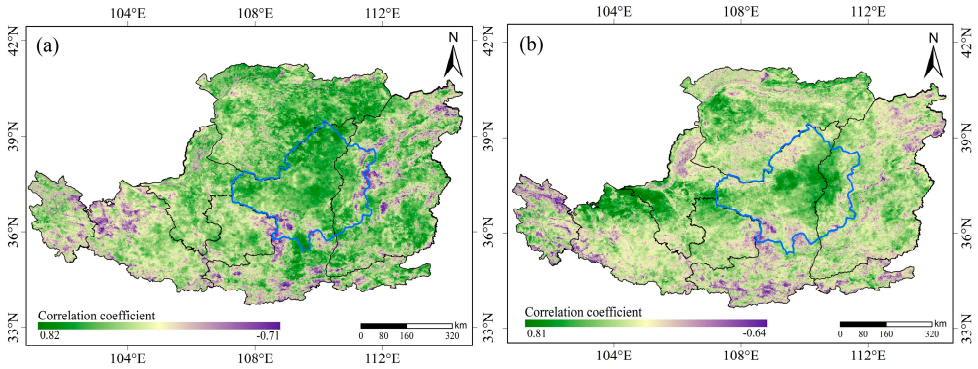

Figure 12. The spatial patterns of correlation coefficients among the NDVI and the climate in the Loess Plateau. (**a**) Temperature, (**b**) Precipitation.

To further analyze the regional differences between the NDVI and the climate in this plateau, the the significance test of the correlation between the annual maximum NDVI and climatic factors in the bioclimatic zone of this plateau was statistically presented in Figure 13. In the Zone GRASS, Zone FOR-GRASS and Zone FOR, the area with significant positive and extremely significant positive correlation between NDVI and temperature was larger than that between NDVI and precipitation. The area with significant positive and extremely significant positive correlation between NDVI and precipitation was larger than that between NDVI and temperature in the Zone DES.

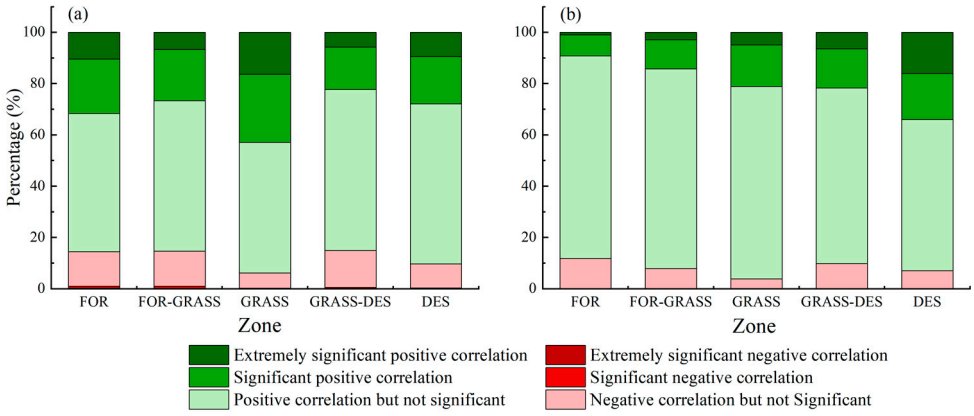

Figure 13. Significance test statistics of NDVI–climate correlation in different bioclimatic zones of the Loess Plateau. (**a**) Temperature, (**b**) Precipitation.

4.6. The Response of NDVI to Human Activities

Figure 14 shows the spatial distribution of NDVI residual trends in the Loess Plateau from 1985 to 2015. The area with an upward trend of residuals accounted for 90.78% of this plateau. Among them, the area that showed a significant upward trend accounted for 62.87%, which was mainly centralized in the key zone of the GGP and the eastern Gansu. The area with a downward trend of residuals accounted for 9.92% of this plateau, which was located around the cities of Xi'an in the south, Taiyuan in the northeast, Yinchuan in the northwest, and Xining in the west.

We quantified the contribution of climatic factors and human activities to the NDVI based on residual analysis. The results showed that the contribution of climatic factors to the NDVI was 34.78%, and the contribution of human activities to the NDVI was 65.22%. Among them, the area with the contribution of climatic factors to the NDVI increase in the range of 25–50% was the largest, accounting for 63.47%. This was mainly found in eastern Inner Mongolia, western Ningxia Shaanxi, and parts of Shanxi (Figure 15a). The area with

the contribution of climatic factors to the NDVI decrease in the range of 0–25% was the largest, accounting for 44.60%. This was mainly distributed in Qinghai, northern Ningxia, northern Shanxi in southern Shaanxi, and northeastern Inner Mongolia (Figure 15c).

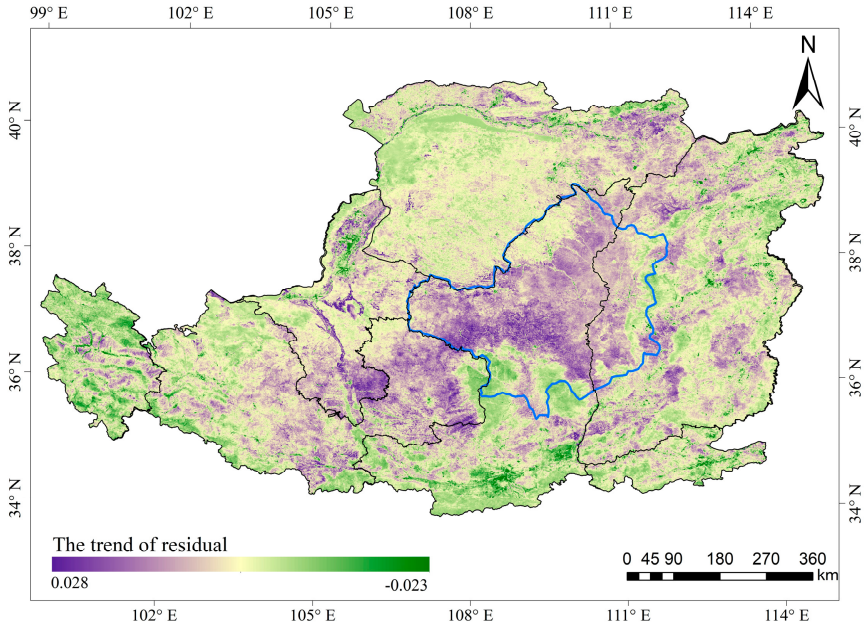

Figure 14. The spatial distribution of NDVI residual trends in the Loess Plateau.

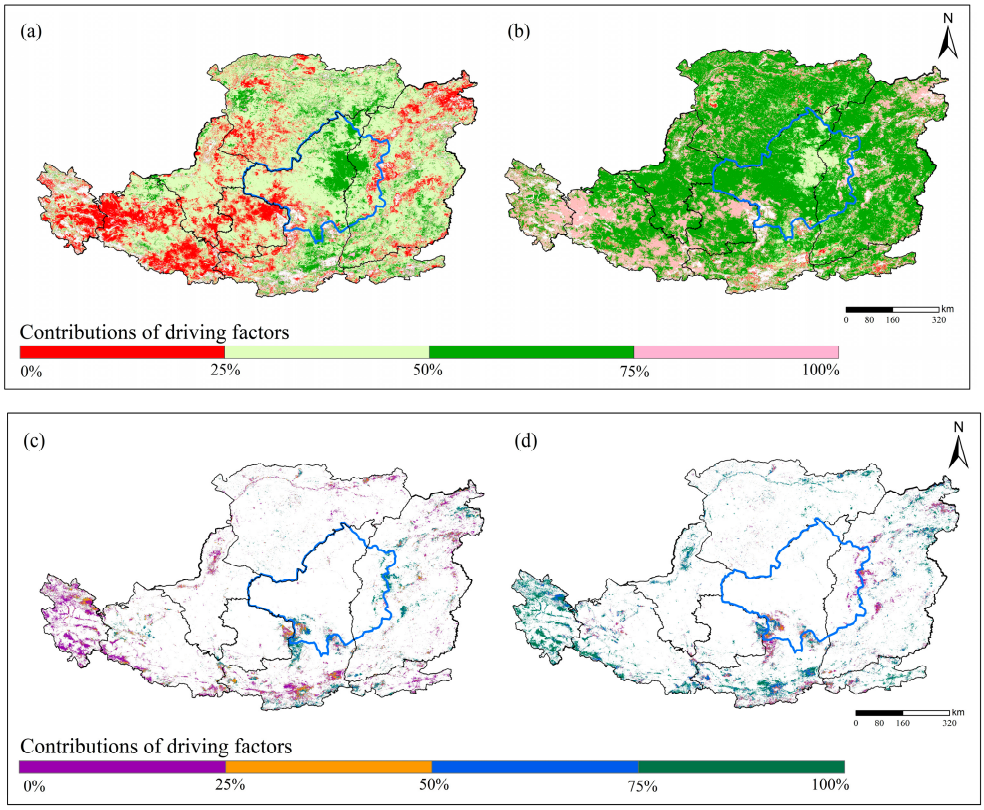

Figure 15. The distribution of the contribution of climate change and human activities to the NDVI changes. (**a**,**b**) is the distribution of the contribution of climate change and human activities to the NDVI increase, (**c**,**d**) is the distribution of the contribution of climate change and human activities to the NDVI decrease.

The area with the contribution of human activities to the NDVI increase in the range of 50–75% was the largest, accounting for 63.47%. This was distributed in Ningxia, Inner Mongolia, Shanxi, and northern Shaanxi (Figure 15b). The area with the contribution of human activities to the NDVI decrease in the range of 75–100% was the largest, accounting for 44.56%. This was mainly distributed in Qinghai, northern Ningxia, northern Shanxi in southern Shaanxi, and northeastern Inner Mongolia. It was mainly found in Xining, Xi'an, Yinchuan, Hohhot, and other urban areas (Figure 15d).

5. Discussion

5.1. Variation in Characteristics of NDVI under Different Topographies

Topographic factors remarkably influence the spatial distribution characteristics of the NDVI by affecting the water, heat, and nutrients. Previous studies have shown the complexities of the influence of topography on the NDVI distribution. The topographic factors affecting the NDVI are diverse in different regions [26]. Furthermore, the effect of the same topographic factor on the NDVI distribution differs in different places [27]. The NDVI was strongly influenced by elevation and slope in the Yangtze River basin [28]. Elevation was the principal factor in influencing the distribution of the NDVI in the Three Parallel Rivers Region and the Southeast Qinghai-Tibet Plateau [29]. The greatest growth rate in the NDVI was found when the elevations were between 1600 m and 1800 m, and the slopes were between 3° and 5° in Taihang Mountain [30]. Moreover, this was also found when the elevation was between 500 m and 1000 m and the slope was between 6° and 16° in the Hanjiang River Basin [31]. This demonstrated the linkage between NDVI distribution and elevation and slope in the Loess Plateau.

The change in elevation not only directly affects the reallocation of materials and energy, such as humidity and heat, but it also affects the frequency of human activities, which vertically zoned the growth of vegetation [32]. When the elevation was below 500 m, the natural conditions and available nutrients were more favorable. However, the area of the NDVI reduction accounted for 8% of this region, which was larger than the area with elevations of 500–1000 m and 1000–1500 m. We can find that the area with elevations below 500 m occupied by cultivated land and construction land accounted for 68.95% and 15.15%, respectively, by overlaying land use with elevation statistics. Human activities destroyed more vegetation, resulting in a larger area showing a downward trend in the NDVI when the elevation was below 500 m. When the elevation was between 1500 m and 3000 m, human activities decreased as the elevation increased. The GGP was started in this area to expand the area where the NDVI showed an upward trend. When the elevation was above 3000 m, the area showed an upward trend of the NDVI decreasing sharply. Precipitation decreases, and temperature decreases as elevation rises from the southeast to northwest in the Loess Plateau. This was the main reason for the decrease in the NDVI within the region.

The slope represents the steepness of the terrain. It determines the occurrence of soil erosion by influencing natural conditions, such as surface runoff, soil infiltration, and soil thickness, which have an impact on vegetation growth [27]. The area with slopes ranging from 0° to 5° was flat, which served as an important area for human activities and urban construction. These activities severely damaged the vegetation, resulting in a larger area that showed a downward trend in the NDVI. The areas with slopes of 6–15° and 15–25° were the main areas where the policy of GGP required measures to be taken, resulting in a relatively larger area that showed the extremely significant upward trend in the NDVI. When the slope exceeded about 25°, the area of the NDVI reduction increased. The reasons may include two aspects. On the one hand, as the slope increases, soil infiltration decreases, slope runoff decreases, soil erosion increases, and nutrient loss increases. On the other hand, the increasing slope decreases the temperature and precipitation.

5.2. Response of the NDVI to Climate and Human Activities in Different Bioclimatic Zones

From Table 4, it was found that the contribution of human activities to the NDVI was higher in Zone FOR, Zone FOR-GRASS, Zone GRASS, and Zone GRASS-DES than in Zone

DES. Among them, the contribution of human activities to the NDVI decrease in Zone FOR and Zone GRASS-DES was higher than its contribution to the NDVI increase (Figure 16). The main reason was that the two sub-zones contained major urban areas, such as Xi'an, Xining, and Hohhot, with concentrated populations and rapid urbanization. Woodlands and grasslands were mostly converted to construction land, and the surrounding vegetation has been damaged to some extent. These resulted in a larger area with a downward trend in NDVI in this region (Figure 17). It indicated that the negative effect of human activities, such as urban expansion, on vegetation recovery was more obvious. In Zone FOR-GRASS and Zone GRASS, the contribution of human activities to the NDVI increase was higher than its contribution to the NDVI decrease. Because of the inclusion of the key zone of the GGP and the better water and heat conditions in the area, the NDVI in these two sub-zones had a larger area with an upward trend. This demonstrated the positive effect of the ecological restoration project on the NDVI increase, which was in accordance with the results of Liu et al. [33]. In Zone DES, the intensity of human activity was low. Climate was the major factor influencing the NDVI in this zone.

Overall, the contribution of human activities to the NDVI was more pronounced in this plateau than that of the climatic factors to NDVI, accounting for 65.22%. However, the result of Li et al. for this plateau was 55% [34]. The differences in the study results may be related to the differences in the duration of time and the type of NDVI data taken.

Table 4. The contribution of climatic factors and human activities to NDVI changes in different bioclimatic zones.

Zone	Contribution/%	
	Climatic Factor	Human Activities
FOR	33.87	66.13
FOR-GRASS	37.56	62.44
GRASS	35.28	64.72
GRASS-DES	33.79	66.21
DES	44.69	55.31

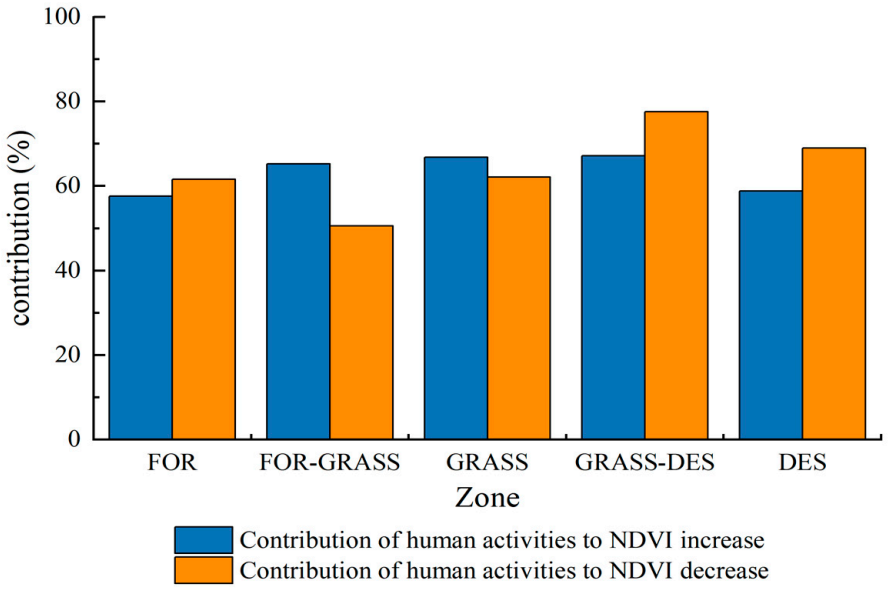

Figure 16. The contribution of human activities to NDVI changes in different bioclimatic zones.

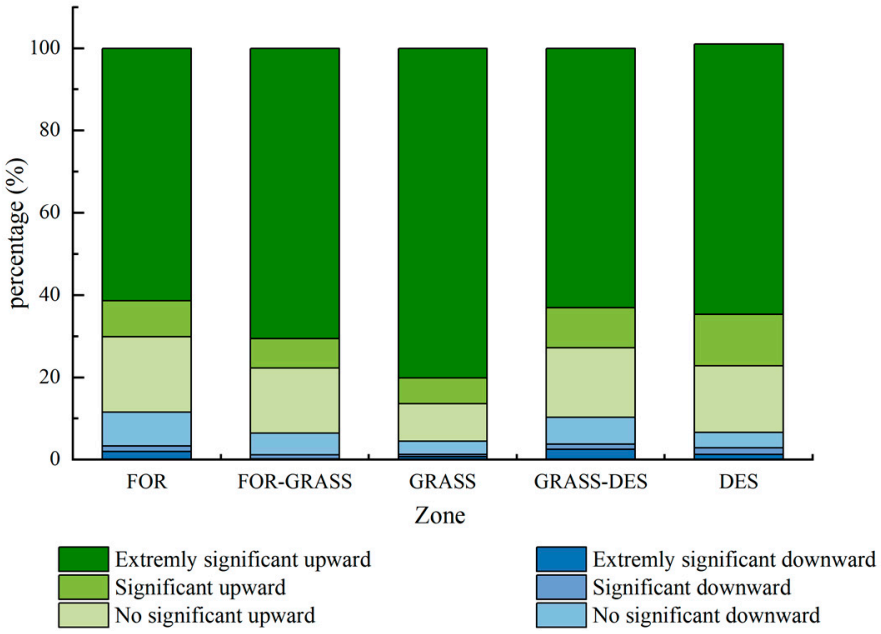

Figure 17. Significance test statistics of NDVI trend in different bioclimatic zones of the Loess Plateau from 1985 to 2015.

6. Conclusions

We analyzed the spatio-temporal patterns of the NDVI and its influencing factors in the Loess Plateau over the past 31 years using the new NDVI data. The main findings were as follows:

1. The ESTARFM data fusion model retains more spatial information. Furthermore, the correlation between the fused data and the original MODIS NDVI was high ($R^2 = 0.93$, $p < 0.01$), which can meet the needs of subsequent studies.
2. The annual average NDVI of this plateau ranged from 0.027 to 0.973, with a zonal distribution and a gradual increase from the northwest to the southeast. The annual maximum NDVI in the study area manifested a significant upward trend from 1985 to 2015, and the growth rate from 2000 to 2015 (0.0078/a) was higher than that from 1985 to 1999 (0.0008/a). Spatially, the area with an upward trend in the NDVI accounted for 89.48% of this plateau, and it was mainly concentrated in southern Ningxia, eastern Gansu, northern Shaanxi, eastern Inner Mongolia, and parts of Shanxi.
3. There were different patterns between the trends in the NDVI and the topographic factors in the study area. The larger area with the extremely significant upward trend of NDVI was found in elevations of 500–1500 m, with slopes of 6–15°. The larger area with the extremely significant downward trend in the NDVI was found at elevations higher than 3000 m, with slopes greater than 35°.
4. The effect of the NDVI and climatic factors manifested remarkable regional differences in the Loess Plateau, specifically from the northwest to the southeast NDVI, where the correlation with precipitation decreased and correlation with temperature increased. The average correlation coefficients of temperature and precipitation with the annual maximum NDVI were 0.24 and 0.22, respectively, with 31.81% and 18.05% of the area significantly correlated. Overall, the effect of the temperature on the NDVI was greater than that of the precipitation.
5. Overall, the contribution of human activities to the NDVI changes was greater than that of the climatic factors (65.22% for human activities and 34.78% for climatic factors). Among them, the area with a higher contribution of human activities to the NDVI increase was located in Zone FOR-GRASS and Zone GRASS, which was highly consistent with the area where the GPP was implemented. This showed the positive effect of ecological construction projects on the recovery of regional vegetation. The

area with a high contribution of human activities to the NDVI decrease was located in Zone FOR and Zone GRASS-DES, which was distributed in line with the provincial capital city such as Xining, Yinchuan, Xi'an, and Hohhot. This revealed that the negative effects of human activities, such as municipal expansion, on vegetation were also more evident.

The findings provided scientific evidence for the assessment and sustainability of the ecology in the Loess Plateau. We also provided a new perspective for studying the NDVI variations in large-scale areas with complex topographies. However, the factors affecting the NDVI were complex. The choice of climate factors may be incomplete when we use residual analysis to build the regression equation of climate and NDVI. Future studies should consider more comprehensively the various factors (e.g., solar radiation, etc.) and conduct in-depth studies on how to quantitatively calculate the contribution of different factors to the NDVI.

Author Contributions: X.F. performed the data analyses and wrote the manuscript; P.G. helped perform the analyses with constructive discussions; B.T. provided the references for the research methodology; C.W. contributed to the data analyses; X.M. contributed to the conception of the study. All authors have read and agreed to the published version of the manuscript.

Funding: This research was funded by the National Natural Science Foundation of China (42277354; U2243211).

Data Availability Statement: The data presented in this study are available and contained within the article.

Acknowledgments: Acknowledgement for the data support from the "Loess Plateau SubCenter", National Earth System Science Data Center, National Science & Technology Infrastructure of China. (http://loess.geodata.cn (accessed on 2 January 2023))".

Conflicts of Interest: The authors declare no financial or scientific conflict of interest.

References

1. Tong, X.; Wang, K.; Brandt, M.; Yue, Y.; Liao, C.; Fensholt, R. Assessing future vegetation trends and restoration prospects in the karst regions of southwest China. *Remote Sens.* **2016**, *8*, 357. [CrossRef]
2. Li, H.; Xie, M.; Wang, H.; Li, S.; Xu, M. Spatial heterogeneity of vegetation response to mining activities in resource regions of northwestern China. *Remote Sens.* **2020**, *12*, 3247. [CrossRef]
3. Ning, T.; Liu, W.; Lin, W.; Song, X. NDVI variation and its responses to climate change on the northern Loess Plateau of China from 1998 to 2012. *Adv. Meteorol.* **2015**, *2015*, 725427. [CrossRef]
4. Zhu, Y.; Zhang, J.; Zhang, Y.; Qin, S.; Shao, Y.; Gao, Y. Responses of vegetation to climatic variations in the desert region of northern China. *Catena* **2019**, *175*, 27–36. [CrossRef]
5. Zhao, A.; Zhang, A.; Liu, J.; Feng, L.; Zhao, Y. Assessing the effects of drought and "Grain for Green" Program on vegetation dynamics in China's Loess Plateau from 2000 to 2014. *Catena* **2019**, *175*, 446–455. [CrossRef]
6. Murat, A.; Zhang, X.P.; Chen, L.L.; Lin, P.F.; Sun, Y.P. Spatial-temporal distribution of desertification on the Loess Plateau using GIMMS NDVI data. *J. Soil Water Conserv.* **2015**, *13*, 24–31.
7. Fu, B.; Liu, Y.; Lü, Y.; He, C.; Zeng, Y.; Wu, B. Assessing the soil erosion control service of ecosystems change in the Loess Plateau of China. *Ecol. Complex.* **2011**, *8*, 284–293. [CrossRef]
8. Usman, M.; Liedl, R.; Shahid, M.A.; Abbas, A. Land use/land cover classification and its change detection using multi-temporal MODIS NDVI data. *J. Geogr. Sci.* **2015**, *25*, 1479–1506. [CrossRef]
9. He, Y.; Lee, E.; Warner, T.A. A time series of annual land use and land cover maps of China from 1982 to 2013 generated using AVHRR GIMMS NDVI3g data. *Remote Sens. Environ.* **2017**, *199*, 201–217. [CrossRef]
10. Pan, X.; Gao, Y.; Wang, J. The inversion research of land desertification in Alxa Banner based on normalized difference vegetation index. *Chin. J. Soil Sci.* **2018**, *49*, 1024–1033.
11. Li, G.Y.; Chen, S.S.; Yan, Y.; Yu, C. Effects of urbanization on vegetation degradation in the Yangtze River Delta of China: Assessment based on SPOT-VGT NDVI. *J. Urban Plan. Dev.* **2015**, *141*, 05014026. [CrossRef]
12. Zhang, Y.; Ye, A. Spatial and temporal variations in vegetation coverage observed using AVHRR GIMMS and Terra MODIS data in the mainland of China. *Int. J. Remote Sens.* **2020**, *41*, 4238–4268. [CrossRef]
13. Gao, F.; Masek, J.; Schwaller, M.; Hall, F. On the blending of the Landsat and MODIS surface reflectance: Predicting daily Landsat surface reflectance. *IEEE Trans. Geosci. Remote Sens.* **2006**, *44*, 2207–2218.

14. Yin, Q.; Liu, M.; Cheng, J.; Ke, Y.; Chen, X. Mapping paddy rice planting area in northeastern China using spatiotemporal data fusion and phenology-based method. *Remote Sens.* **2019**, *11*, 1699. [CrossRef]
15. Hilker, T.; Wulder, M.A.; Coops, N.C.; Linke, J.; McDermid, G.; Masek, J.G.; Gao, F.; White, J.C. A new data fusion model for high spatial-and temporal-resolution mapping of forest disturbance based on Landsat and MODIS. *Remote Sens. Environ.* **2009**, *113*, 1613–1627. [CrossRef]
16. Zhu, X.; Chen, J.; Gao, F.; Chen, X.; Masek, J.G. An enhanced spatial and temporal adaptive reflectance fusion model for complex heterogeneous regions. *Remote Sens. Environ.* **2010**, *114*, 2610–2623. [CrossRef]
17. Knauer, K.; Gessner, U.; Fensholt, R.; Kuenzer, C. An ESTARFM fusion framework for the generation of large-scale time series in cloud-prone and heterogeneous landscapes. *Remote Sens.* **2016**, *8*, 425. [CrossRef]
18. Wu, M.; Zheng, N.; Wang, C. Assessing the accuracy of spatial and temporal image fusion model of complex area in South China. *Int. J. Geogr. Inf. Sci.* **2014**, *16*, 776–783.
19. Xiao, J. Satellite evidence for significant biophysical consequences of the"Grain for Green" Program on the Loess Plateau in China. *J. Geophys. Res. Biogeosci.* **2014**, *119*, 2261–2275. [CrossRef]
20. Li, P.; Wang, J.; Liu, M.; Xue, Z.; Bagherzadeh, A.; Liu, M. Spatio-temporal variation characteristics of NDVI and its response to climate on the Loess Plateau from 1985 to 2015. *Catena* **2021**, *203*, 105331. [CrossRef]
21. Sun, Q.; Liu, C.; Chen, T.; Zhang, A. A weighted-time-lag method to detect lag vegetation response to climate variation: A case study in Loess Plateau, China, 1982–2013. *Remote Sens.* **2021**, *13*, 923. [CrossRef]
22. Feng, X.; Fu, B.; Lu, N.; Zeng, Y.; Wu, B. How ecological restoration alters ecosystem services: An analysis of carbon sequestration in China's Loess Plateau. *Sci. Rep.* **2013**, *3*, 2846. [CrossRef]
23. Zhao, A.; Yu, Q.; Wang, D.; Zhang, A. Spatiotemporal dynamics of ecosystem water use efficiency over the Chinese Loess Plateau base on long-time satellite data. *Environ. Sci. Pollut. Res.* **2022**, *29*, 2298–2310. [CrossRef] [PubMed]
24. Peng, J.; Liu, Z.; Liu, Y.; Wu, J.; Han, Y. Trend analysis of vegetation dynamics in Qinghai–Tibet Plateau using Hurst Exponent. *Ecol. Indic.* **2012**, *14*, 28–39. [CrossRef]
25. Bai, Y. Analysis of vegetation dynamics in the Qinling-Daba Mountains region from MODIS time series data. *Ecol. Indic.* **2021**, *129*, 108029. [CrossRef]
26. Walsh, S.J.; Crawford, T.W.; Welsh, W.F.; Crews-Meyer, K.A. A multiscale analysis of LULC and NDVI variation in Nang Rong district, northeast Thailand. *Agric. Ecosyst. Environ.* **2001**, *85*, 47–64. [CrossRef]
27. Xiong, Y.; Wang, H. Spatial relationships between NDVI and topographic factors at multiple scales in a watershed of the Minjiang River, China. *Ecol. Inform.* **2022**, *69*, 101617. [CrossRef]
28. Deng, Y.; Yao, S.; Hou, M.; Zhang, T. Temporal and Spatial Variation of Vegetation NDVI and Its Topographic Differentiation Effect in the Middle and Upper Reaches of the Yangtze River Basin. *Resour. Environ. Yangtze Basin.* **2020**, *29*, 66–78.
29. Wang, C.; Wang, J.; Naudiyal, N.; Wu, N.; Cui, X.; Wei, Y.; Chen, Q. Multiple effects of topographic factors on Spatio-temporal variations of vegetation patterns in the three parallel rivers region, Southeast Qinghai-Tibet Plateau. *Remote Sens.* **2021**, *14*, 151. [CrossRef]
30. Hu, S.; Wang, F.Y.; Zhan, C.S.; Zhao, R.X.; Mo, X.G.; Liu, L.M.Z. Detecting and attributing vegetation changes in Taihang Mountain, China. *J. Mt. Sci.* **2019**, *16*, 337–350. [CrossRef]
31. Liu, H.; Zheng, L.; Yin, S. Multi-perspective analysis of vegetation cover changes and driving factors of long time series based on climate and terrain data in Hanjiang River Basin, China. *Arab. J. Geosci.* **2018**, *11*, 509. [CrossRef]
32. Sun, W.; Song, X.; Mu, X.; Gao, P.; Wang, F.; Zhao, G. Spatiotemporal vegetation cover variations associated with climate change and ecological restoration in the Loess Plateau. *Agric. For. Meteorol.* **2015**, *209*, 87–99. [CrossRef]
33. Liu, Z.; Wang, J.; Wang, X.; Wang, Y. Understanding the impacts of 'Grain for Green'land management practice on land greening dynamics over the Loess Plateau of China. *Land Use Policy* **2020**, *99*, 105084. [CrossRef]
34. Li, J.; Peng, S.; Li, Z. Detecting and attributing vegetation changes on China's Loess Plateau. *Agric. For. Meteorol.* **2017**, *247*, 260–270. [CrossRef]

Disclaimer/Publisher's Note: The statements, opinions and data contained in all publications are solely those of the individual author(s) and contributor(s) and not of MDPI and/or the editor(s). MDPI and/or the editor(s) disclaim responsibility for any injury to people or property resulting from any ideas, methods, instructions or products referred to in the content.